

Tomographic imaging of ratiometric fluorescence resonance energy transfer in scattering media

Yi Zhang,¹ Xu Cao,¹ Yanyan Xu,¹ Qing Liu,¹ Yue Zhang,¹ Jianwen Luo,^{1,2}
Xiaodong Liu,¹ and Jing Bai^{1,*}

¹Department of Biomedical Engineering, School of Medicine, Tsinghua University, Beijing 100084, China

²Center for Biomedical Imaging Research, Tsinghua University, Beijing 100084, China

*Corresponding author: deabj@tsinghua.edu.cn

Received 3 January 2012; revised 4 May 2012; accepted 4 June 2012;
posted 6 June 2012 (Doc. ID 160728); published 11 July 2012

A method to visualize and quantify fluorescence resonance energy transfer (FRET) in scattering media is proposed. It combines the ratiometric FRET method with fluorescence molecular tomography (FMT) in continuous wave (CW) mode. To evaluate the performance of the proposed method, experiments on a tissue-mimicking phantom are carried out. The results demonstrate that the proposed approach is capable of visualizing and quantifying the FRET distribution in scattering media, which implies the further application of the ratiometric assay in *in vivo* studies. © 2012 Optical Society of America

OCIS codes: 170.6960, 170.3010, 170.6280, 170.3880.

1. Introduction

In recent years, more and more attention has been focused on fluorescence resonance energy transfer (FRET). FRET is a near-field mechanism by which nonradiative energy is transferred from an excited molecular fluorophore (donor) to the adjacent chromophore (acceptor) via dipole–dipole coupling [1–4]. Because the degree of the FRET strongly depends on the distance between donor and acceptor, this technology can be used to reveal the spatial proximity relationship between the two fluorescence-labeled sites [2]. With the development of the FRET pair proteins, at present, FRET has been widely applied to study the biological processes, for example, protein–protein interactions [5–7], protein–DNA interactions [8], intracellular calcium dynamics [9–12], and protease activities [13,14].

Generally, the measurement of FRET is mainly based on two methods, namely fluorescence lifetime imaging microscopy (FLIM) [15,16] and ratiometric microscopy. Although FLIM is more accurate and

insensitive to artifacts, it requires specialized light sources and detectors, which complicate the experimental measurements [4,7]. In contrast, the ratiometric method is simpler and easier to use. As one of the ratiometric methods, the three-cube FRET method [9–12,17] has been widely used to evaluate the FRET. In this method, the fluorescence images are firstly acquired using three sets of filters, namely the donor channel, the acceptor channel, and the FRET channel. Then, based on these acquired images, the FRET ratio (FR) is calculated, which is used as an indicator to evaluate the degree of FRET. As demonstrated in [9,17], the three-cube FRET method can not only avoid sophisticated fluorophore concentration measurements but is also fast and nondestructive. In spite of these advantages, currently, the three-cube method is only applied to the microscopic level due to the high degree of light scattering in scattering media.

In this paper, we extend the three-cube FRET method from the microscopic to macroscopic level by combining the technology of fluorescence molecular tomography (FMT) [18–20]. Similar to [9], the intensities of the fluorescent proteins are first measured and reconstructed in the three channels

(the donor channel, the acceptor channel, and the FRET channel). Second, using the reconstructed intensities of the proteins, the FR is calculated to evaluate the degree of FRET. With the generated FR, we image the three-dimensional (3D) distribution of FRET at the macroscopic level. To demonstrate the capacity of the proposed method, phantom experiments are performed on a free-space FMT imaging system. The experimental results demonstrate that FRET distribution in the phantom can be localized and quantified with this approach.

This paper is organized as follows. The proposed method is presented in Section 2. In Section 3, experiments on the tissue-mimicking phantom are conducted to evaluate the proposed method. In Section 4, phantom results are shown. Finally, we make some discussions about this study in Section 5.

2. Methods

A. Fluorescence Reconstruction

The fluorescence tomography images are obtained by using the FMT algorithm in continuous wave (CW) mode [18–20]. In a highly scattering medium, the photon propagation can be modeled using the diffusion equation coupled with the Robin-type condition [21]:

$$\begin{cases} -\nabla \cdot [D(r)\nabla G(r)] + \mu_a(r)G(r) = \delta(r - r_s) & r \in \Omega \\ 2qD(r)\frac{\partial G(r)}{\partial \vec{n}} + G(r) = 0 & r \in \partial\Omega \end{cases} \quad (1)$$

where Ω denotes the domain of the problem, $\partial\Omega$ denotes the boundary, $D(r)$ is the diffusion coefficient, $\mu_a(r)$ is the absorption coefficient, q is a constant depending upon the optical reflective index mismatch at the boundary, and \vec{n} denotes the outward normal vector to the boundary. For FMT with point illumination, a point source is usually modeled as an isotropic source $\delta(r - r_s)$, where r_s is the point-one transport mean free path into the medium from the illumination spot. The diffusion equation is solved by the finite element method. After obtaining the Green's functions, the forward model of FMT can be written as a linear system [19,22]:

$$\phi_{fl} = \mathbf{W}n, \quad (2)$$

where ϕ_{fl} is the measured fluorescence signal by the detectors, \mathbf{W} is the weight matrix, and n is the fluorescence yielded to be reconstructed. The unknown n is obtained by solving Eq. (2) using algebraic reconstruction technique (ART) [23] with nonnegative constraints.

B. Three-Cube Method

The three-cube method is used to correct for the spectral cross talk of the donor and acceptor by employing three different sets of filters, namely the donor channel, the acceptor channel, and the FRET channel

Table 1. Three Channels and Corresponding Filters

Channel	Excitation Filter	Emission Filter
CFP (Donor)	440 ± 5 nm	480 ± 5 nm
YFP (Acceptor)	500 ± 5 nm	530 ± 5 nm
FRET	440 ± 5 nm	530 ± 5 nm

(Table 1). In this paper, the used donor and acceptor are respectively cyan fluorescent protein (CFP) and yellow fluorescent protein (YFP).

To further understand the principle of the three-cube method, the spectrum of the dimer of CFP and YFP (referred to as the C–Y dimer) is shown in Fig. 1(a), which is the superposition of the CFP and YFP spectra. The C–Y dimer representing a CFP–YFP concatemer, in which CFP and YFP are held within 100 Å, shows FRET [right panel in

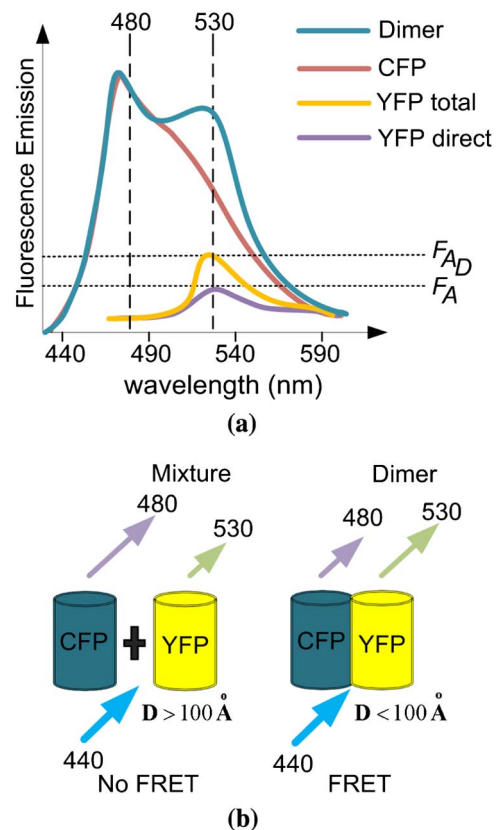


Fig. 1. (Color online) Illustration of the principle of the three-cube method. (a) Fluorescence emission spectrum with the excitation light at 440 nm. Emission at 530 nm (dimer curve) is the sum of CFP emission (CFP curve) and YFP emission (YFP total curve). A portion of its YFP emission is due to FRET, and the rest is due to direct excitation. Similarly, for the mixture, the emission at 530 nm is the sum of CFP emission (CFP curve) and YFP emission (YFP direct curve). Its YFP emission (YFP direct curve) is due only to direct excitation. The spectra are adapted from [9]; (b) comparison between the two used samples. The length of the arrow represents the relative intensity of emission fluorescence for particular wavelength. CFP and YFP in the mixture are held outside of 100 Å. CFP and YFP in the C–Y dimer are held within 100 Å. The two samples are illuminated by the same excitation light with a wavelength of 440 nm.

Fig. 1(b)]. Because of FRET, the YFP emission F_{Ad} [YFP total curve in Fig. 1(a)] in the C–Y dimer encounters an emission increase compared with that of the direct YFP emission F_A [YFP direct curve in Fig. 1(a)] near 530 nm. On the contrary, the mixture of CFP and YFP (referred to as the mixture), obtained from blending the CFP sample with the YFP sample, shows no FRET as the distance between CFP and YFP is more than 100 Å [left panel in Fig. 1(b)]. Thus its YFP emission F_A [YFP direct curve in Fig. 1(a)] is only the result of direct excitation, leading to a lower spectrum near 530 nm compared with that of the dimer F_{Ad} . Thus FRET can be then quantified by the FR, which is a unitless index equal to the fractional increase in YFP emission due to FRET, expressed as [9]

$$FR = \frac{F_{Ad}}{F_A} = \frac{S_{\text{FRET}}(DA) - R_{D1} \cdot S_{\text{CFP}}(DA)}{R_{A1} \cdot [S_{\text{YFP}}(DA) - R_{D2} \cdot S_{\text{CFP}}(DA)]}, \quad (3)$$

where R_{D1} , R_{D2} , and R_{A1} are constants obtained from the calibration samples (CFP, YFP) for system correction with $R_{D1} = S_{\text{FRET}}(D)/S_{\text{CFP}}(D)$, $R_{D2} = S_{\text{YFP}}(D)/S_{\text{CFP}}(D)$, and $R_{A1} = S_{\text{FRET}}(A)/S_{\text{YFP}}(A)$. $S_{\text{CFP}}(D)$, $S_{\text{YFP}}(D)$, and $S_{\text{FRET}}(D)$ are the reconstructed intensities of the CFP sample (donor) in the CFP, YFP, and FRET channels (Table 1), respectively. $S_{\text{YFP}}(A)$ and $S_{\text{FRET}}(A)$ are the reconstructed intensities of the YFP sample (acceptor) in the YFP and FRET channels, respectively. When the FR of the mixture is calculated, $S_{\text{CFP}}(DA)$, $S_{\text{YFP}}(DA)$, and $S_{\text{FRET}}(DA)$ in Eq. (3) denote the reconstructed intensities of the mixture in the CFP, YFP, and FRET channels, respectively. When the FR of the dimer is calculated, $S_{\text{CFP}}(DA)$, $S_{\text{YFP}}(DA)$, and $S_{\text{FRET}}(DA)$ indicate the reconstructed intensities of the C–Y dimer in the three channels, respectively.

When the FR equals 1, there is no FRET. When the FR is above 1, there is FRET, and the FR bears a linear relation to the degree of FRET [9–12,17]. With higher degree of FRET, higher FR can be obtained. After the reconstructions of fluorescence intensities in the three channels, the distribution of the FRET in scattering media is obtained by calculating the FR pixel by pixel using Eq. (3).

Based on Eq. (3) and [9], in the calculation of FR, the experimental factors, such as the concentrations of donor and acceptor, the excitation power, the characteristics of the optical filters, the fluorescence intensity, and the autofluorescence, have been considered. That is, the above experimental factors could not affect the evaluation of FRET.

3. Phantom Experiments

A. Sample Preparation

Cultures of transformed HEK 293 T cells were maintained in Dulbecco's Modified Eagle Medium (DMEM) supplemented with 10% fetal bovine serum in a humidified atmosphere containing 5% CO₂ at 37 °C. HEK 293 T cells were transfected respectively

with the CFP, YFP, and C–Y dimer cDNA plasmids by Lipofectamine 2000 (Invitrogen, California, USA). The transfection methods yielded transfection efficiency greater than 80%. Briefly, HEK 293 T cells were plated at a density of 2×10^6 cells per 100 mm Corning dish and transfected the following day. For Lipofectamine 2000 transfections, HEK 293 T cells were transfected with 8 μg of CFP, YFP, and C–Y dimer plasmid cDNA, respectively, and 20 μL of Lipofectamine per plasmid in 500 μL of Optimem⁻¹ per dish for 6 h according to the manufacturer's specifications. After transfection with Lipofectamine, the cells were washed and maintained in DMEM supplemented with 10% fetal bovine serum. After 48 h of transfection, HEK293 T cells were lysed using phenylmethylsulfonyl fluoride (PMSF) and protease inhibitors. The cell lysates were centrifugalized to remove the membrane fragments and were finally assessed with a Zeiss confocal microscope (LSM-710, Zeiss, Oberkochen, Germany) at excitation light of 440 nm and emission light of 530 nm. After the above procedures, the CFP sample, YFP sample, and C–Y dimer sample were obtained.

In the paper, two different samples, namely the mixture and the C–Y dimer, were tested in the experiments to evaluate the proposed method. The mixture was obtained from blending the CFP sample with the YFP sample and was used as a control assessment for the C–Y dimer. In contrast, the C–Y dimer, representing a CFP–YFP concatemer, was obtained from the cell transfection and lysate as described above. In the C–Y dimer [right panel in Fig. 1(b)], as the distance of CFP and YFP is less than 100 Å, the energy is transferred from the excited CFP to the nearby YFP via dipole–dipole coupling. In the mixture [left panel in Fig. 1(b)], as the CFP is more than 100 Å away from the YFP, almost no energy will be transferred between CFP and YFP. Thus the relative YFP emission in the C–Y dimer is larger than that in the mixture, which is due to the FRET [17,24].

B. Experimental Setup

The overview of the noncontact, free-space FMT system is illustrated in Fig. 2, similar to our previously developed system [25]. It consisted of a 300 W xenon lamp (Max-302, Asahi Spectra, CA, USA), a fiber, a rotation stage, a 512 × 512 pixel electron-multiplying charge-coupled device (EMCCD) camera (iXon DU-897, Andor Technologies, Belfast, Northern Ireland), a 35 mm $f/1.6D$ lens (C3514-M, PENTAX, Tokyo, Japan) coupled to the EMCCD camera, and a filter wheel with emission filters fixed on it.

The excitation and emission filters used in the donor (CFP), acceptor (YFP), and FRET channels are listed in Table 1. The xenon lamp, containing a filter wheel itself, tunable from 200 to 1200 nm, was employed as the excitation light source (see excitation filters in Table 1). The fiber attached to the lamp was employed to generate a light spot, which was focused onto the surface of the imaged object. The

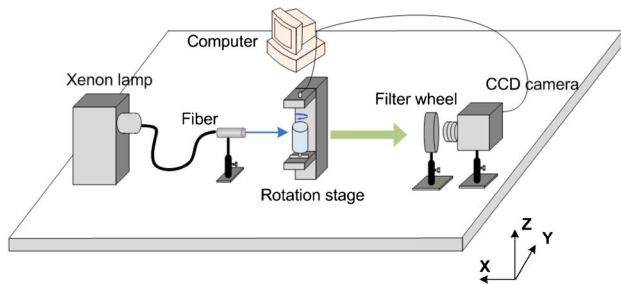


Fig. 2. (Color online) Experimental setup. The setup consists of a xenon lamp as the excitation light, a fiber coupled to the lamp, a stage to perform the rotation of the imaged object, a CCD camera, and a filter wheel containing the filters to capture the corresponding images. The CCD camera and the rotation stage are under the control of a personal computer.

rotation stage was designed for rotating the imaged object around its z axis over 360° at a speed of $6^\circ/\text{s}$. The photons transmitting through the imaged object were detected by the EMCCD camera, which was cooled to -70°C to reduce dark noise. The filter wheel, placed in front of the EMCCD, was utilized in the light path to collect images with different emission filters (see emission filters in Table 1). The selection of the bandpass excitation/emission filters was based on the spectral properties of the used FRET pair proteins. Control of the rotation stage and acquisition of data were manipulated by customized software written in LabWindows (National Instruments, Austin, TX, USA).

C. Phantom Experiments

In order to verify the capability of the proposed method in imaging FRET in scattering media, phantom experiments were performed on the FMT imaging system. A glass cylinder (outer diameter ~ 3.0 cm) containing 1% intralipid was employed to mimic scattering properties of tissue, with an absorption coefficient μ_a of 0.022 cm^{-1} and a reduced scattering coefficient μ'_s of 17.0 cm^{-1} when using blue excitation light [26,27]. A transparent glass tube (outer diameter ~ 0.4 cm) was immersed in the tissue-mimicking phantom [Fig. 3(a)], approximately 1.0 cm to the boundary of the phantom [Fig. 3(b)]. The glass tube was alternatively filled with the same dose ($50\ \mu\text{L}$) of the tested samples, that is, the mixture and the C–Y dimer. The excitation light and the center of the imaged proteins were at the same height, approximately 2.6 cm from the bottom of the phantom [Fig. 3(b)].

To eliminate the background noise, endogenous protein obtained from lysates of the nonfluorescent cells was first imaged in the experiment. CFP and YFP samples were also imaged in the experiment as the calibration samples for system correction. For each sample (endogenous protein, CFP, YFP, mixture, and C–Y dimer), fluorescence images were collected in the CFP, YFP, and FRET channels, respectively (Table 1), typically utilizing 24 projections with an angular increment of 15° . For each

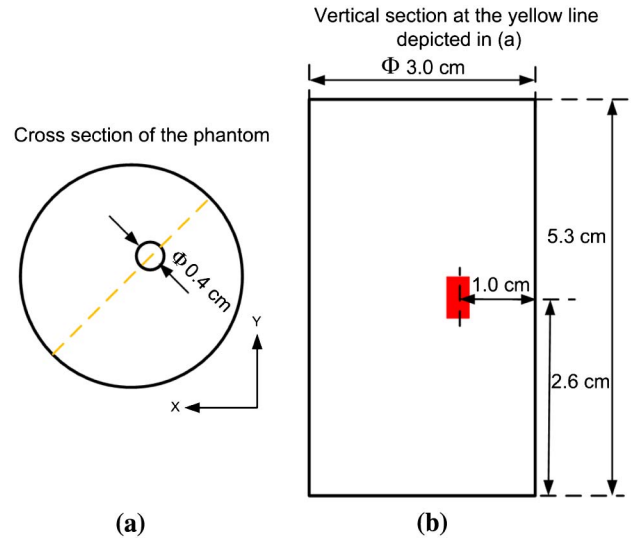


Fig. 3. (Color online) Illustration of the tissue-mimicking phantom. (a) Cross section of the phantom; (b) Vertical section at the yellow dashed line depicted in (a). The employed phantom is a glass cylinder (outer diameter ~ 3.0 cm) containing 1% intralipid ($\mu_a = 0.022\text{ cm}^{-1}$, $\mu'_s = 17.0\text{ cm}^{-1}$ when using blue excitation light). A transparent glass tube (outer diameter ~ 0.4 cm) alternatively filled with $50\ \mu\text{L}$ endogenous protein sample, CFP sample, YFP sample, mixture sample, and C–Y dimer sample is immersed at the position about 1.0 cm to the boundary of the phantom.

projection, an image of 512×512 pixels was obtained with an exposure time of 0.3 s and a CCD gain of 5. All fluorescence images of the four samples, that is, CFP, YFP, mixture, and C–Y dimer, were background corrected by subtracting the images of the endogenous protein pixel by pixel in the corresponding three channels. To recover the 3D surface of the phantom, 72 white-light images were captured with an angular increment of 5° .

4. Results

A. Reconstruction of Fluorescent Proteins

Reconstructed images (Fig. 4) show the distribution of the CFP sample, the YFP sample, the mixture sample, and the C–Y dimer sample in the CFP, YFP, and FRET channels, respectively, in which the CFP and YFP samples are used for system calibration. All the tomographic images (Fig. 4) are in the same slice of the phantom where the red, outer circle depicts the boundary of the phantom and the blue, inner circle depicts the actual positions of the proteins. The reconstructed position of each protein matches its actual position well. These results are shown in the same color scale, facilitating the comparison of each sample in the three channels. It is evident that the fluorescence intensities of YFP (the second row in Fig. 4) differ from channel to channel. Signal in the YFP channel is much stronger than that in the other two channels, in good agreement with the assessment of living cells by microscopy (not shown). All the samples share a similarity in that their relative reconstructed fluorescence

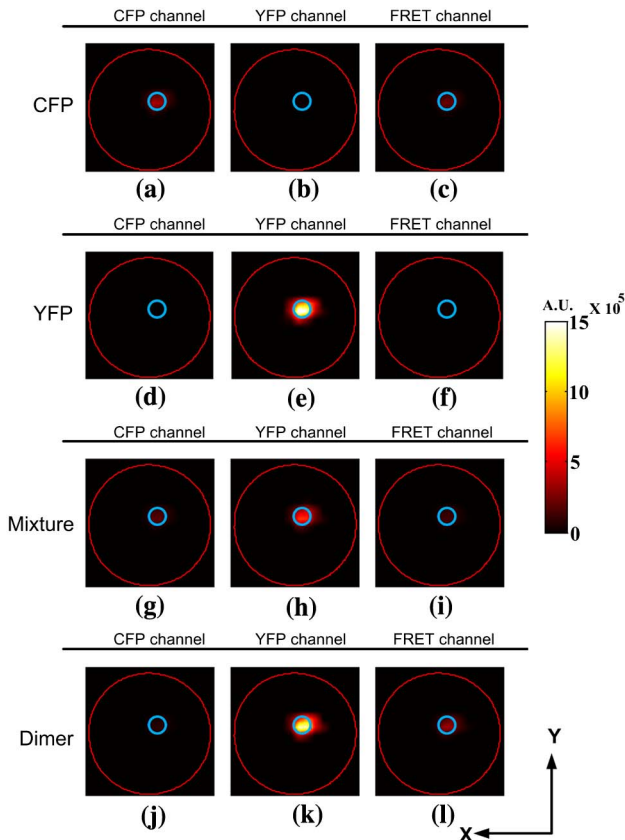


Fig. 4. (Color online) Results of the fluorescence reconstruction. (a)–(c) Tomographic images of CFP sample in (a) CFP channel, (b) YFP channel, and (c) FRET channel; (d)–(f) tomographic images of YFP sample in the three channels; (g)–(i) tomographic images of the mixture sample in the three channels. (j)–(l) Tomographic images of C–Y dimer sample in the three channels. All the images, depicted in the same color scale, are taken from the same slice of the phantom. The red, outer circle depicts the boundary of the phantom, and the blue, inner circle depicts the actual position of the proteins.

intensities in the three channels correlate well with the assessment by microscopy (not shown).

B. Reconstruction of the FRET

In a manner analogous to the microscopic imaging, the degree of FRET was quantified by the FR, a ratio between total YFP emission and direct YFP emission [Eq. (3)]. After the reconstructions of fluorescence intensities in the three channels, the FR of each tested sample (the mixture and the C–Y dimer) was calculated pixel by pixel using Eq. (3). The 3D FRET distributions of the mixture and the dimer are presented in Fig. 5, demonstrating the capacity of the proposed method to image FRET distribution in the phantom. The two-dimensional (2D) tomographic images (right panel in Fig. 5) are taken at the slices depicted in the 3D images (red circle in left panel of Fig. 5). The FR of the mixture [Fig. 5(a)] appears to be ~ 1 , suggesting no FRET, as the distance between CFP and YFP in the mixture is greater than 100 \AA . As expected, because of the proximity of CFP to YFP in the dimer ($< 100 \text{ \AA}$), the FR of the

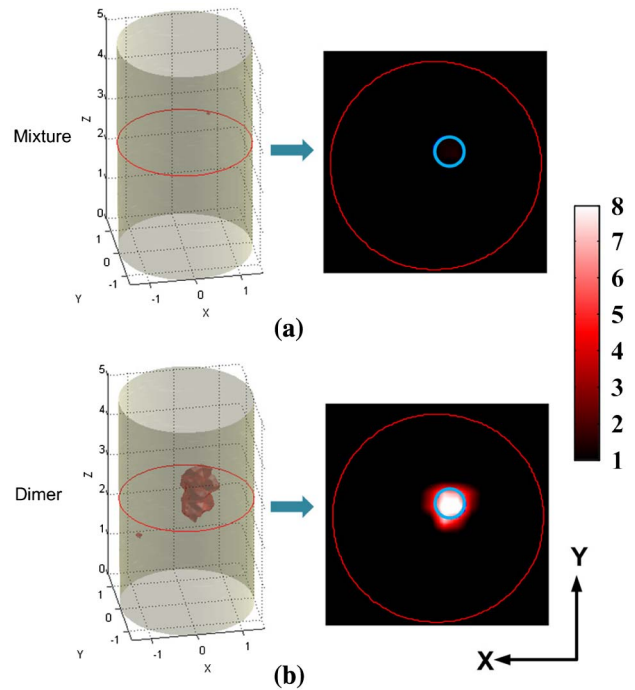


Fig. 5. (Color online) Reconstruction results of the FRET distribution. (a) 3D (left panel) and 2D (right panel) FRET distribution of the mixture; (b) 3D (left panel) and 2D (right panel) FRET distribution of the dimer. The FR of the mixture (~ 1) is much smaller than that of the dimer (~ 7).

dimer [Fig. 5(b)] shows a much higher value than that of the mixture, yielding ~ 7 . In addition, the reconstructed position of each sample agrees well with its actual position (blue, inner circle in Fig. 5). The procedures and results in this paper are similar to those obtained from the microscopic three-cube method [9,17].

5. Discussion

The development of FRET provides researchers with crucial insights into biological mechanisms and physiological functions of cells. With regard to the importance of FRET in biological studies, it is urgent to obtain the distribution of FRET at the macroscopic level.

In this paper, we proposed a method combining the ratiometric three-cube assay with the FMT in CW mode. To evaluate the capability of this proposed method, phantom experiments were performed on the FMT imaging system. After reconstructing the fluorescence intensities in the three channels (Table 1), the FRET distributions were obtained by calculating the FR, which represented the fractional enhancement of YFP due to FRET. The results show that the combination of the ratiometric three-cube method with the technology of FMT in CW mode can offer an approach to localizing and quantifying FRET in scattering media.

There are several limitations in this study. First, it should be pointed out that in this paper, the FR is utilized as an indicator to evaluate the degree of

FRET. Several experimental factors (e.g., the concentrations of donor and acceptor, the excitation power, the characteristics of the optical filters, the fluorescence intensity, the autofluorescence), have been considered in the calculation of FR [9]. In other words, using the three-cube method, the above experimental factors could not affect the evaluation of FRET. Nevertheless, when the FRET pair (CFP/YFP pair) is applied to the *in vivo* study, if the above factors (e.g., the autofluorescence) are corrected using proper correction techniques, it would improve the FMT reconstruction quality, which could be helpful to the calculation of FR. In addition, considering the penetration of light in biological tissues, the FRET pair used in the study may have limitations in the *in vivo* study. This problem, to some extent, can be improved by some techniques such as the use of optical clearing agents [28]. Also, the FRET pairs of longer wavelengths may be helpful to the *in vivo* study, for the penetration into tissues would be deeper and the autofluorescence in tissues would be lower. Finally, only tissue-mimicking phantoms were employed in the experiments to verify the feasibility of the proposed method. *In vivo* experiment should be considered in future work.

To sum up, by combining the three-cube FRET method with the technology of FMT, we resolve the 3D distribution of FRET at the macroscopic level. Future work will be focused on its *in vivo* applications.

We would like to thank Professor Zhijie Chang (School of Medicine, Tsinghua University, China) for the HEK293 T cells and Professor David Yue (School of Medicine, Johns Hopkins University, USA) for the CFP, YFP, and C–Y dimer cDNA. This work is supported by the National Basic Research Program of China (973) under grant no. 2011CB707701; the National Major Scientific Instrument and Equipment Development Project under grant no. 2011YQ030114; the National Natural Science Foundation of China under grant nos. 81071191, 60831003, 30930092, 30872633, and 81171382; the Beijing Natural Science Foundation under grant no. 3111003; and the Tsinghua-Yue-Yuen Medical Science Foundation, the Tsinghua University Key Faculty Support Plan under grant no. 413406009.

References

1. T. Förster, "Zwischenmolekulare energiewanderung und fluoreszenz," *Ann. Phys.* **437**, 55–75 (1948).
2. K. Truong and M. Ikura, "The use of FRET imaging microscopy to detect protein-protein interactions and protein conformational changes *in vivo*," *Curr. Opin. Struct. Biol.* **11**, 573–578 (2001).
3. M. Elangovan, H. Wallrabe, Y. Chen, R. N. Day, M. Barroso, and A. Periasamy, "Characterization of one- and two-photon excitation fluorescence resonance energy transfer," *Methods* **29**, 58–73 (2003).
4. J. Yuan, L. Peng, B. E. Bouma, and G. J. Tearney, "Quantitative FRET measurement by high-speed fluorescence excitation and emission spectrometer," *Opt. Express* **18**, 18839–18851 (2010).
5. D. W. Piston and G. J. Kremers, "Fluorescent protein FRET: the good, the bad and the ugly," *Trends Biochem. Sci.* **32**, 407–414 (2007).
6. R. Hallworth, B. Currall, G. Michael, M. G. Nichols, X. Wu, and J. Zuo, "Studying inner ear protein-protein interactions using FRET and FLIM," *Brain Research* **1091**, 122–131 (2006).
7. C. Banning, J. Votteler, D. Hoffmann, H. Koppensteiner, M. Warmer, R. Reimer, F. Kirchhoff, U. Schubert, J. Hauber, and M. Schindler, "A flow cytometry-based FRET assay to identify and analyse protein-protein interactions in living cells," *PLoS One* **5**, e9344 (2010).
8. A. Gansen, A. Valeri, F. Hauger, S. Felekyan, S. Kalinin, K. Tótha, J. Langowska, and C. A. M. Seidelb, "Nucleosome disassembly intermediates characterized by single-molecule FRET," *Proc. Natl. Acad. Sci. USA* **106**, 15308–15313 (2009).
9. M. G. Erickson, B. A. Alseikhan, B. Z. Peterson, and D. T. Yue, "Preassociation of calmodulin with voltage-gated Ca²⁺ channels revealed by FRET in single living cells," *Neuron* **31**, 973–985 (2001).
10. X. Liu, P. S. Yang, W. Yang, and D. T. Yue, "Enzyme-inhibitor-like tuning of Ca²⁺ channel connectivity with calmodulin," *Nature* **463**, 968–972 (2010).
11. M. G. Erickson, H. Liang, M. X. Mori, and D. T. Yue, "FRET two-hybrid mapping reveals function and location of L-type Ca²⁺ channel CaM preassociation," *Neuron* **39**, 97–107 (2003).
12. P. S. Yang, B. A. Alseikhan, H. Hiel, L. Grant, M. X. Mori, W. Yang, P. A. Fuchs, and D. T. Yue, "Switching of Ca²⁺-dependent inactivation of Ca_v1.3 channels by calcium binding proteins of auditory hair cells," *J. Neurosci.* **26**, 10677–10689 (2006).
13. Y. Y. Hsu, Y. N. Liu, W. Wang, F. J. Kao, and S. H. Kung, "In vivo dynamics of enterovirus protease revealed by fluorescence resonance emission transfer (FRET) based on a novel FRET pair," *Biochem. Biophys. Res. Commun.* **353**, 939–945 (2007).
14. T. Kohl, K. G. Heinze, R. Kuhlemann, A. Koltermann, and P. Schwille, "A protease assay for two-photon cross-correlation and FRET analysis based solely on fluorescent proteins," *Proc. Natl. Acad. Sci. USA* **99**, 12161–12166 (2002).
15. V. Gaiand, S. Kularatne, P. S. Low, and K. J. Webb, "Deep-tissue imaging of intramolecular fluorescence resonance energy-transfer parameters," *Opt. Lett.* **35**, 1314–1316 (2010).
16. J. McGinty, D. W. Stuckey, V. Y. Soloviev, R. Laine, M. Wylezinska-Arridge, D. J. Wells, S. R. Arridge, P. M. W. French, J. V. Hajnal, and A. Sardini, "In vivo fluorescence lifetime tomography of a FRET probe expressed in mouse," *Biomed. Opt. Express* **2**, 1907–1917 (2011).
17. M. R. Tadross, S. A. Park, B. Veeramani, and D. T. Yue, "Robust approaches to quantitative ratiometric FRET imaging of CFP/YFP fluorophores under confocal microscopy," *J. Microsc.* **233**, 192–204 (2009).
18. X. Liu, D. Wang, F. Liu, and J. Bai, "Principal component analysis of dynamic fluorescence diffuse optical tomography images," *Opt. Express* **18**, 6300–6314 (2010).
19. X. Liu, F. Liu, Y. Zhang, and J. Bai, "Unmixing dynamic fluorescence diffuse optical tomography images with independent component analysis," *IEEE Trans. Med. Imaging* **30**, 1591–1604 (2011).
20. X. Liu, X. Guo, F. Liu, Y. Zhang, H. Zhang, G. Hu, and J. Bai, "Imaging of indocyanine green perfusion in mouse liver with fluorescence diffuse optical tomography," *IEEE Trans. Biomed. Eng.* **58**, 2139–2143 (2011).
21. M. Schweiger, S. R. Arridge, M. Hiraoka, and D. T. Delpy, "The finite element method for the propagation of light in scattering media: boundary and source conditions," *Med. Phys.* **22**, 1779–1792 (1995).
22. D. Wang, X. Liu, and J. Bai, "Analysis of fast full angle fluorescence diffuse optical tomography with beam-forming illumination," *Opt. Express* **17**, 21376–21395 (2009).
23. A. Kak and M. Slaney, *Computerized Tomographic Imaging* (IEEE, 1987).
24. Q. Liu, Y. Zhang, X. Xie, Y. Xu, Y. Zhang, X. Liu, J. Bai, and X. Liu, "Characterization of quantitative FRET sensors for fluorescent molecular tomography," presented at the

Biophysics Society Annual Meeting, Baltimore, Maryland, March 2011.

25. F. Liu, X. Liu, D. Wang, B. Zhang, and J. Bai, "A parallel excitation based fluorescence molecular tomography system for whole-body simultaneous imaging of small animals," *Ann. Biomed. Eng.* **38**, 3440–3448 (2010).
26. S. T. Flock, S. L. Jacques, B. C. Wilson, W. M. Star, and M. J. van Gemert, "Optical properties of intralipid: a phantom medium for light propagation studies," *Lasers Surg. Med.* **12**, 510–519 (1992).
27. R. Michels, F. Foschum, and A. Kienle, "Optical properties of fat emulsions," *Opt. Express* **16**, 5907–5925 (2008).
28. R. Cicchi, D. Sampson, D. Massi, and F. Pavone, "Contrast and depth enhancement in two-photon microscopy of human skin *ex vivo* by use of optical clearing agents," *Opt. Express* **13**, 2337–2344 (2005).